Journal of Alloys and Compounds 825 (2020) 153865

Contents lists available at ScienceDirect

Journal of Alloys and Compounds

journal homepage: http://www.elsevier.com/locate/jalcom

Structured $La_{0.6}Sr_{0.4}Co_{0.2}Fe_{0.8}O_{3-\delta}$ cathode with large-scale vertical cracks by atmospheric laminar plasma spraying for IT-SOFCs

Yue-Peng Wang , Sen-Hui Liu , Hui-Yu Zhang , Cheng-Xin Li *, Shan-Lin Zhang , Guan-Jun Yang , Chang-Jiu Li

State Key Laboratory for Mechanical Behavior of Materials, School of Materials Science and Engineering, Xi'an Jiaotong University, Xi'an, Shaanxi Province, 710049, PR China

ARTICLE INFO

Article history:
Received 7 November 2019
Received in revised form
13 January 2020
Accepted 14 January 2020
Available online 3 February 2020

Keywords:
Plasma spraying
Coatings
Laminar plasma spraying
Solid oxide fuel cells
Vertical cracks

ABSTRACT

$La_{0.6}Sr_{0.4}Co_{0.2}Fe_{0.8}O_{3-\delta}$ (LSCF) is a promising cathode material for solid oxide fuel cells (SOFCs). Hence, structured LSCF coatings were deposited in this study by atmospheric laminar plasma spraying (ALPS) at the spraying distances from 150 mm to 250 mm. Particles with high temperature were obtained at low plasma arc power of only 15 kW. The microstructural characterization of the coatings showed cluster-like morphologies on the top surfaces and columnar features with large-scale vertical cracks at the cross section. An evolution mechanism of the coatings was proposed based on particle size. The movement of particles during laminar plasma jet depended on particle size, which was studied experimentally and by simulation to explain the selective deposition. The coatings showed lower polarization resistance when compared to LSCF coatings deposited by atmospheric plasma spraying (APS) due to large vertical crack densities. The high output performance of the SOFCs with the LSCF cathode also proved this phenomenon. The results suggest that ALPS provides extensive options for SOFCs manufacturing.

1. Introduction

$La_{0.6}Sr_{0.4}Co_{0.2}Fe_{0.8}O_{3-\delta}$ (LSCF) material possesses high ionic and electronic conductivities [1], which could reach 70 and 320 S/cm at 700 °C, respectively [2]. LSCF material is usually used as oxygen permeation membranes [3] and solid oxide fuel cells (SOFCs) cathodes [4]. In addition, LSCF is employed in intermediate temperature SOFCs (IT-SOFCs), due to its excellent chemical and thermal stabilities. The mixed ionic–electronic conducting (MIEC) material LSCF allows oxygen to be reduced over a large portion of the electrode surface, effectively promoting cathodic reaction kinetics and reducing the polarization loss [5]. However, further applications of LSCF are still limited by interface reaction features [6] and poor surface catalytic performances [7]. At co-sintering temperatures above 900 °C, LSCF would react with yttria stabilized zirconia (YSZ) to generate $SrZrO_3$ with low conductivity [8]. Therefore, a diffusion barrier layer is usually used during high-temperature sintering. For instance, Szymczewska et al. [9] used $Ce_{0.8}Gd_{0.2}O_{2-\delta}$ (CGO) diffusion barrier layer (DBL) to prevent the interface reactions and reduce cell resistance lose by two orders of magnitude when compared to cells without CGO layer. However, the introduction of DBL challenged the fabrication process and exacerbated the ohmic loss of the cells. Hence, avoiding the formation of low conductivity phase without DBL is still problematic and requires solutions for sintering process.

Plasma spraying (PS) is efficient and inexpensive to deposit coatings. During PS process, elemental diffusion and interface reaction become limited since high temperature sintering is not required. This makes PS suitable for mass production of metal-supported solid oxide fuel cells (MS-SOFCs) [10]. Inside sprayed coatings, numerous voids exist with well-distributed non-bonded interfaces and vertical cracks distributed. Such pores can be useful for diffusion. Furthermore, plasma spraying can be used to control the microstructure and composition of coatings by adjusting the spraying parameters and powder design [11–13].

Atmospheric laminar plasma spraying is a newly developed PS technology possessing a long laminar plasma jet with length up to 700 mm [14]. Moreover, ALPS could lead to better structural uniformity for applications in SOFCs, such as corrugated cells due to longer deposition range. In addition, coatings could be deposited under lower plasma torch power due to the decreasing of air

* Corresponding author. Address: School of Materials Science and Engineering, Xi'an Jiaotong University, State Key Laboratory for Mechanical Behavior of Materials, Xi'an, Shaanxi, 710049, PR China.
E-mail address: licx@mail.xjtu.edu.cn (C.-X. Li).

https://doi.org/10.1016/j.jallcom.2020.153865
0925-8388/

entrainment in the plasma jet and the increasing of heating time. Therefore, laminar plasma spraying is economical and practical for industrial production. However, only few studies suggested the use of laminar plasma in coating deposition. Recently, Liu et al. [15] fabricated thermal barrier coatings with a great number of vertical cracks by laminar plasma spraying. For cathode coating preparation, vertical cracks could benefit oxygen transportation. Furthermore, vertical cracks could enhance the cathode mass transportation and decrease cathode polarization resistance of the coatings.

In this study, novel structured LSCF coatings were fabricated by ALPS to yield coatings with large vertical cracks at different spray distances. The microstructures of the as-obtained coatings were evaluated by various analytical methods and deposition behaviors were analyzed. The deposited units showed preferential distributions at certain distances. The performance of the materials as cathodes of SOFCs were evaluated by electrochemical impedance spectroscopy, and the effect of vertical cracks in coatings on the mass transportation and polarization resistance were discussed.

2. Experimental

2.1. Procedures and materials

A laminar plasma spraying equipment (ZH-30, Zhenhuo Plasma Technology Company, Chengdu, China) was employed at the working parameters listed in Table 1. The plasma torch power was set to 15.2 kW (I = 100 A). The working gas contained 70% nitrogen and 30% argon in volume at a total gas flow rate of 12 slpm. The long spray distances ranged from 150 mm to 250 mm in this study.

Commercial $La_{0.6}Sr_{0.4}Co_{0.2}Fe_{0.8}O_{3-\delta}$ powders (Metco 6830A, Sulzer Metco, Westbury, USA) were utilized as the feedstock material. Typical morphologies of LSCF powders are shown in Fig. 1(a) and size distributions of the powders in Fig. 1(b). LSCF powders showed essentially lognormal large distributions with characteristic particle size of 19 μm (d_{10}), 41 μm (d_{50}), and 70 μm (d_{90}). The particles were injected into plasma jet by specific gravity-vibration method in the radial direction at injecting mass flow rate of 5.12 g/min.

YSZ pellets with diameter of 20 mm and thickness of 1.5 mm were used as substrates and prepared by grit blasting. The diameter of LSCF coatings was set to 8 mm, resulting in active area of symmetrical half-cell of 0.50 cm^2. LSCF splats were deposited on polished YSZ substrates at different spraying distances (SD). A 3D confocal laser microscope was used to characterize the thickness and diameter of the splats.

Whole cells with the structure of 430L||NiO/ScSZ||ScSZ||LSCF were fabricated. The function layers were all deposited on porous stainless steel substrates by plasma spraying. The preparation parameters of the anode and electrolyte can refer to our previous parameters [16,17]. Atmospheric plasma spraying was used to deposit the anode with the arc power of 36 kW. Very low pressure plasma spraying was used to deposit the electrolyte with the arc power of 60 kW. The anode and cathode coatings of about 30 μm were fabricated. The thickness of ScSZ electrolyte was about 40 μm.

Table 1
Laminar plasma spraying parameters.

Parameter	Value
Arc power/kW	15.2
Arc current/A	100
Arc voltage/V	152
Plasma gas (N_2) flow/slpm	8.4
Plasma gas (Ar) flow/slpm	3.6
Powder feeding rate/g·min^{-1}	5.12(no carrier gas)
Spraying distance/mm	150,200,250
Feed powder	$La_{0.6}Sr_{0.4}Co_{0.2}Fe_{0.8}O_{3-\delta}$

2.2. Characterization

Field emission scanning electronic microscope (FE-SEM, VEGA II, TESCAN, Czech) was used to view the microstructures of LSCF coatings and morphologies of the splats. The crystal phases were identified by X-ray diffraction (XRD-6000, Shimadzu, Japan) with Cu-Kα radiation. The in-flight particles surface temperature and velocity were measured by a DPV-2000 system (Technar Automation Ltd., Canada). 3D confocal laser microscope (VK9700K, KEYENCE Corporation, Japan) was used to analyze the diameter and thickness of splats. Area-specific resistance (ASR) of each electrode was evaluated by electrochemical impedance spectroscopy (EIS) method under air atmosphere. To this end, two Ag pastes were attached to LSCF electrodes as current collectors and impedance spectra data were collected by frequency response analyzer (Solartron 1260) and electrochemical interface analyzer (Solartron 1287). Symmetrical cells were tested at open-circuit voltage with amplitude of 10 mV, temperature range from 600 to 750 °C, and frequencies from 0.01 to 1 MHz. Prior to the measurements, the temperature was held at each point for at least 30 min.

For whole cell testing, 95% H_2−5% H_2O for a total flow of 50 sccm was employed as fuel. On the cathode side, the oxygen from ambient air was used as an oxidant. Current voltage characteristics were recorded at different temperatures at 50 °C intervals.

3. Results

3.1. Characteristic of particles in flight

The length of laminar plasma jet without powders at the working parameters was recorded as 0.3 m while that with powders was >0.4 m (S1). In other words, the addition of powders led to disturbance of the plasma jet. To monitor the state of particles in flight, DPV-2000 system was employed. The distributions of in-flight particle velocity and surface temperature are gathered in Fig. 2. For comparison, particle temperature distributions reported by Harris et al. [18] using APS system (Northwest Mettech Axial III Series 600) were also presented in Fig. 2. Note that the temperature of particles in ALPS was always above the melting point of the LSCF material (~1740 °C) [19] and the critical particle deposition temperature of LSCF (~2100 °C) [18] though the surface temperature of the particle decreases slightly with the increase of spraying distance (Fig. 2). At distances from 150 to 350 mm, particle surface temperature is always above 2600 °C and maximum temperature at 150 mm was identified as 3000 °C. On the other hand, particle surface temperature was still below 2600 °C though the atmospheric plasma torch power used by Harris et al. [18] increased to 66.3 kW. The surface temperature of particles obtained by ALPS was much higher than that by APS, indicating significantly improved heating efficiency of particles by ALPS. However, the velocity of particles in laminar plasma jet was generally about 100 m/s due to lower gas flow rate. This value was much lower than that obtained by APS (more than 200 m/s).

3.2. Characteristics of splats deposited at different standoff distances

In Fig. 3(a)-(c), LSCF splats were deposited on polished YSZ substrates at different spray distances. The splats deposited at 150 mm and 200 mm showed many intra-splat microcracks caused

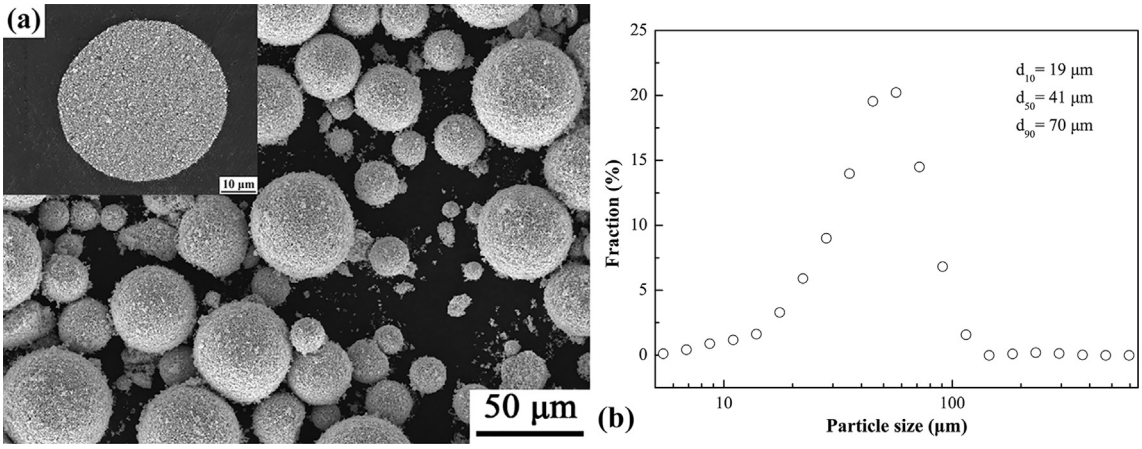

Fig. 1. Characteristics of original powder: (a) Surface morphology and cross-section microstructure. (b) Particle size distribution.

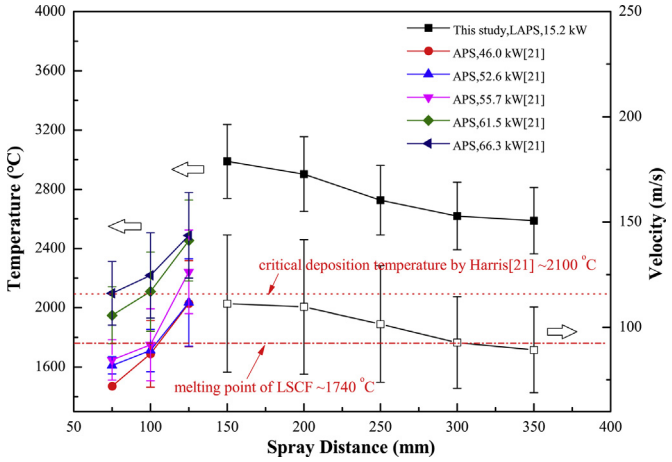

Fig. 2. Particle velocity and particle surface temperature in plasma jet at different positions from the nozzle exit.

by stress during rapid solidification. However, the segment size of splat increased and the number of microcracks decreased significantly at the deposition distance of 250 mm. Intra-splat microcracks are often considered the result of stress release. Therefore, intra-splat microcracks in ceramic splats would be inevitable since the residual tensile stress was much higher than tensile strength [20]. Kuroda et al. [21] recorded a qualitative relationship between residual tensile stress of splats and deposition temperature. The residual tensile stress increased as deposition temperature rose. Qualitatively, the crack pattern could be attributed to the elevated heating effect to substrate by laminar plasma jet. Since laminar plasma technology is used in surface heat treatment [22,23], the deposition temperature of underlying solid can further be influenced by high energy input density plasma jet. Hence, higher tensile stress led to formation of numerous cracks due to superior deposition temperature at spraying distances of 150 mm and 200 mm. The pattern became reversed as spraying distance increased to 250 mm.

Fig. 3(d) presents the flattening ratio of splat and original particle size obtained from statistical data of 300 individual splats at each spraying distance. The flattening ratio of ceramic splats was around 4 among for distances from 150 mm to 250 mm due to the close particle velocity and temperature (Fig. 2). The flattening ratio in ALPS was lower than the value of 5–6 obtained by APS [24] since in-flight particle velocity was much lower. In addition, the original particle size calculated from splat volume increased with spraying distance. The mean particle size ranged from 15 μm to 24 μm, lower than factual size since the effect of original powder porosity was unable to consider in calculation. The data revealed that size of deposition units differed from the spraying distance. At different standoff distances, the powder exhibited selective deposition depending on particle size.

3.3. *Microstructures of LSCF coatings prepared by laminar plasma spraying*

Fig. 4 illustrates the XRD patterns of LSCF coatings obtained at different spray distances. Note that all results were normalized by maximum peak of YSZ substrate. XRD data included the peaks of both coatings and substrates since areas of LSCF coatings were smaller than those of YSZ substrates. As shown in Fig. 4, the as-sprayed coatings maintained perovskite structures. At distances of 150 mm and 200 mm, the coatings presented (110) as preferred orientation. However, the XRD peak positions shifted to high angles, attributed to changes in lattice constant. Using XRD data, the lattice constants of the LSCF coatings at the spraying distances of 150, 200 and 250 mm can be calculated to be 3.85 Å, 3.85 Å, and 3.84 Å, which are well agreement with and slightly smaller than the value in earlier reports (3.86–3.88 Å) [25–27]. The high temperature during plasma spraying process is attributed to oxygen loss occurring in in-flight powder particles [28,29]. The decrease in the lattice constant with the spraying distance might be caused by the further loss of oxygen.

S2(a) displays a typical coating surface morphology obtained at spraying distance of 150 mm. The surface showed splats, top cracks, clusters, and un-melted particles. In marked Region yellow, a cluster deposition was observed, while Region blue displayed fine porous structure with submicron particles. Compared to submicron particles in Region blue, those in Region red showed loose structure and weak bonding with each other, suggesting that formation of clusters. To analyze the chemical composition, EDX scanning was carried out for the region shown in S2(a). In S2(b), the element content ratio of La, Sr, Co and Fe in the deposited coating deposited remained close to 6:4:2:8. According to surface scanning distribution maps, all elements looked evenly distributed on the surface, indicating no significant elemental loss throughout the deposition process.

Fig. 5 shows the surface morphology of LSCF cathodes obtained at different spraying distances. The macroscopic structures of the coatings are exhibited in Fig. 5(a, c, e). As spraying distance rose, the

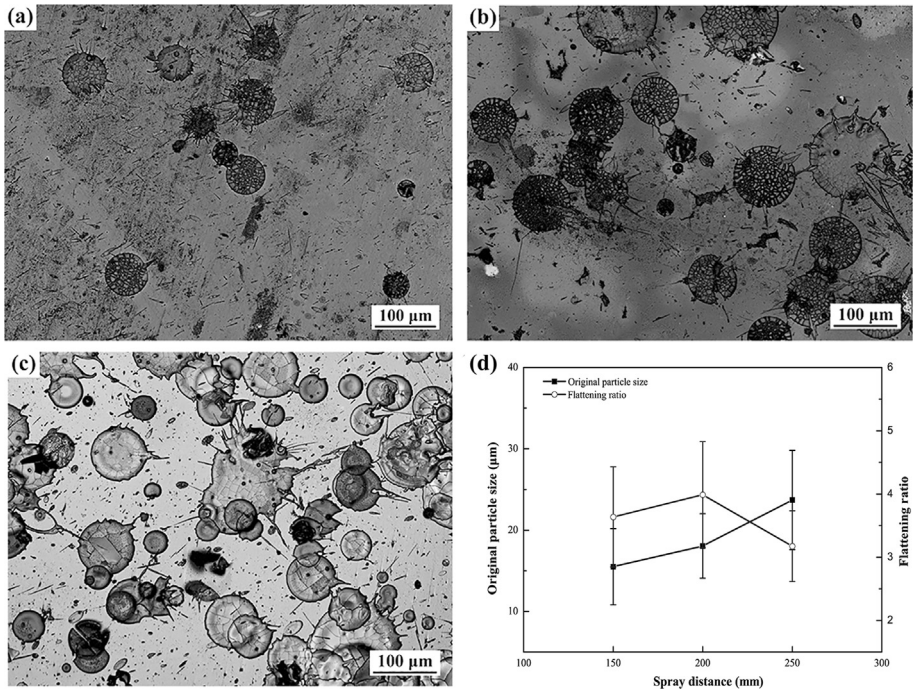

Fig. 3. Characteristics of LSCF splats. Morphologies of splats (a) SD = 150 mm, (b) SD = 200 mm, and (c) SD = 250 mm; (d) flattening ratio and original particle size statistics at different spraying distances.

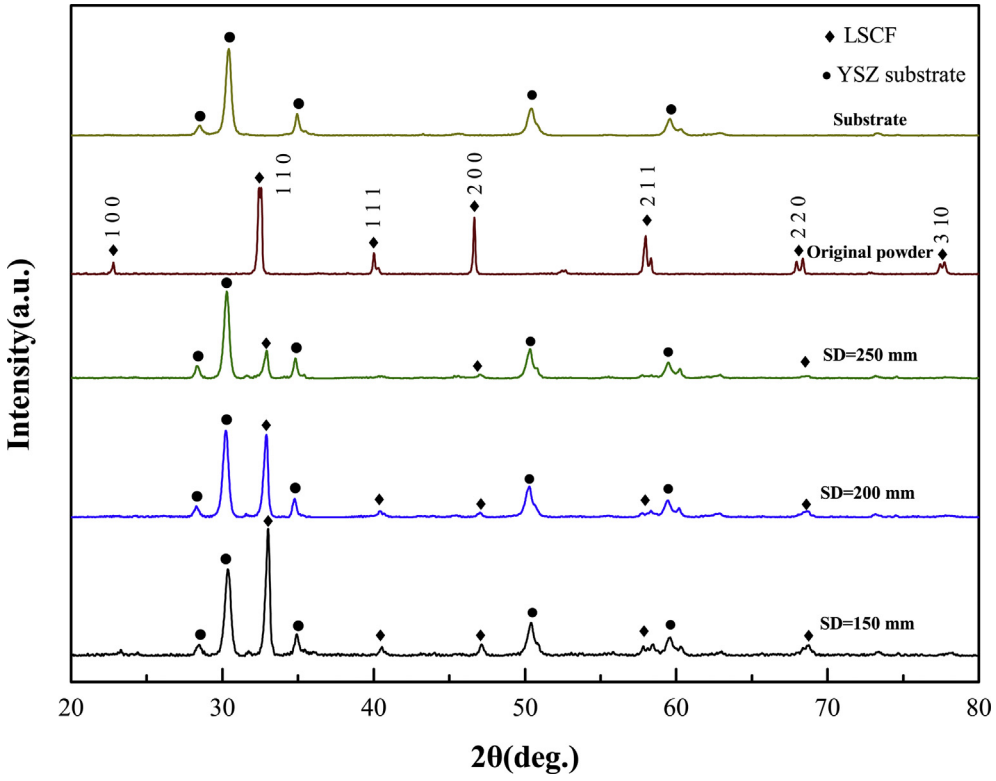

Fig. 4. XRD patterns of LSCF coatings.

number of splats with low flattening rates on surface gradually increased. Fig. 5(b, d, f) illustrate the high magnification morphologies of LSCF coatings. The surface of each coating contained large numbers of nanoclusters, formed by gas phase deposition or powder bursting. The fine structure could facilitate the oxygen reduction reaction.

S3 presents the coating thicknesses calculated from image analysis of coatings deposited under the same parameters. Therefore, the thickness of each coating only depended on the deposition efficiency. The increase in spraying distance led to rapid growth of

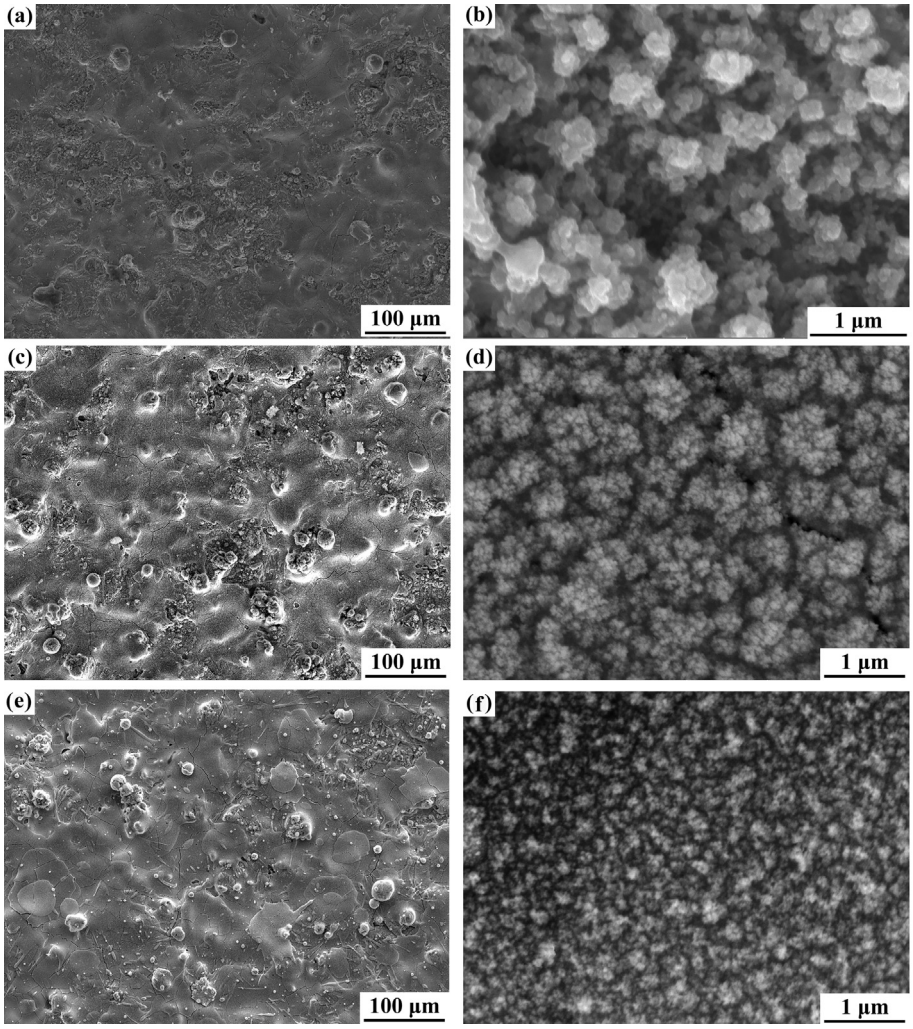

Fig. 5. Surface morphology of LSCF coatings at: (a, b) SD = 150 mm, (c, d) SD = 200 mm, and (e, f) SD = 250 mm.

coating, suggesting that deposition efficiency increased with spraying distance.

Fig. 6(a, b, c) shows images of polished microstructure the fractured morphologies of LSCF coatings. As spraying distance increased, the vertical cracks density decreased. Structures with large numbers of vertical cracks were observed at the spraying distances of 150 mm and 200 mm. However, visible vertical cracks were only few for coatings prepared at spraying distance of 250 mm. Fig. 6(d, e, f) illustrates the fractured morphologies of LSCF coatings. Unlike typical lamellar structures of APS coatings, the coatings tops in Fig. 6(d) and (e) showed columnar structures segmented by vertical cracks. However, typical lamellar structures formed at spraying distance of 250 mm. These fractured morphologies were consistent with the polished microstructure. Vertical cracks were meant to release residual stress due to the thermal gradient during the spraying process. The formation of large-scale segmentation cracks was related to high deposition temperature, enabling microcracks in the first lamellae to propagate and penetrate into the next lamellae and consequently [30,31].

3.4. Cathode polarization resistance

Fig. 7 exhibits the electrochemical impedance spectral data of symmetrical cells with laminar plasma-sprayed LSCF cathodes. To clearly comparing the polarization arcs, high-frequency intercepts were set to zero. The value of polarization resistance (R_p) equals to the difference between the two intercepts of the polarization impedance curve along the real axis. The polarization resistances of cathode coatings deposited at distances of 150, 200 and 250 mm at 750 °C were estimated to 0.33, 0.31 and 0.46 Ω cm^2, respectively. The total polarization resistances of the electrodes fabricated at the distances of 150 mm and 200 mm were much lower than the value of APS coatings reported in the literature (0.541 Ω cm^2) [32]. In S4, the temperature dependence of polarization resistances of LSCF electrodes coatings obtained at various spray distances were plotted as lgR-1000/T. Using Arrhenius relationship, the gradient of the curves could be related to the activation energy. At spraying distances of 150, 200 and 250 mm, the activation energies were 1.36, 1.32 and 1.27 eV, respectively. These values were comparable with reported data [33].

4. Discussion

4.1. Particle movement and selective deposition

During laminar plasma spraying process, the use of the traditional feeder with carrier gas is often challenging. Hence, a gravity

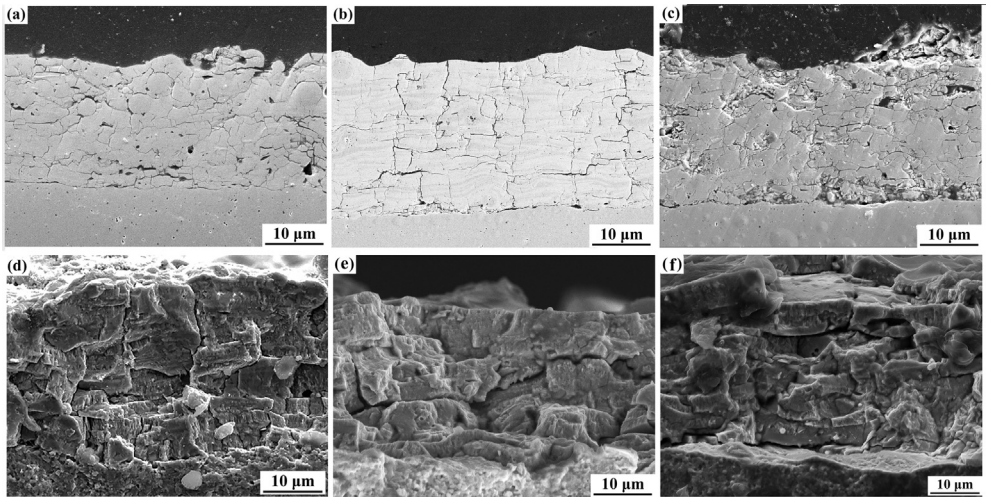

Fig. 6. SEM images of LSCF coatings. Polished microstructure of obtained at (a) SD = 150 mm, (b) SD = 200 mm, and (c) SD = 250 mm; fractured morphologies at (d) SD = 150 mm, (e) SD = 200 mm, and (f) SD = 250 mm.

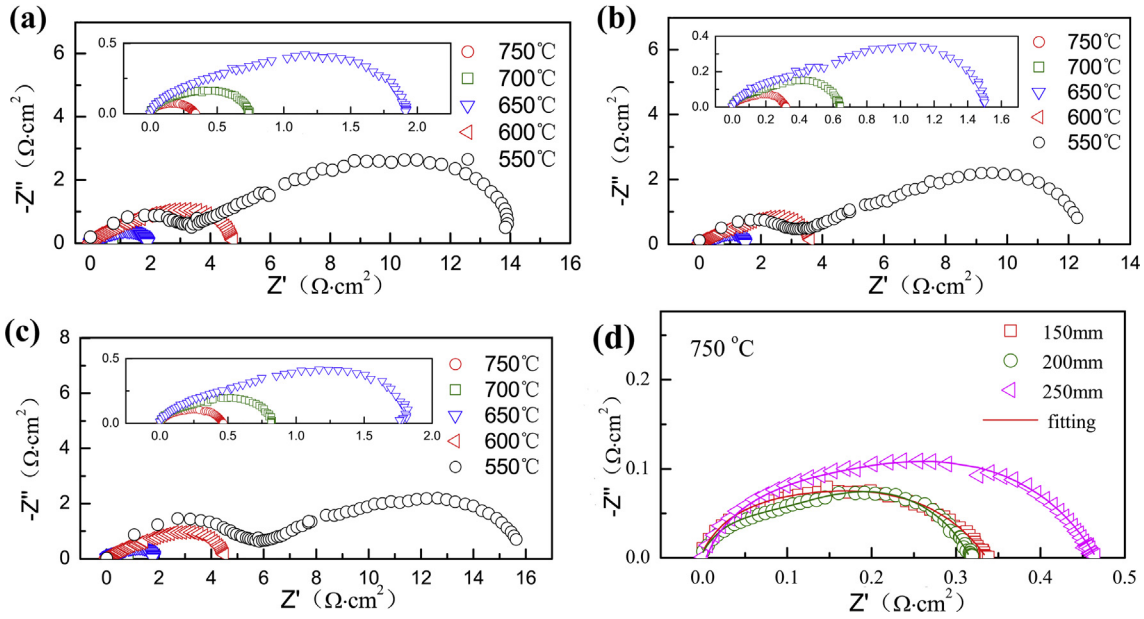

Fig. 7. Electrochemical impedance spectra of LSCF cathode measured under OCV conditions. AC plots at spraying distance of (a) 150 mm, (b) 200 mm, and (c) 250 mm; (d) AC impedance plots of three samples at 750 °C.

feeding device was used to maintain laminar flow state. After injection of particles into the plasma jet, they can be approximated as free sediment in vertical direction. According to Stokes laws, particle with vertical motion in laminar jet will produce a lift force. The viscosity force would be proportional to first order square of particle size. If assuming that Staffman lift force, virtual mass force and Basset force can be ignored in laminar flow, the force of particles in vertical direction can be express by Eq. (1) [34]:

$$\frac{\pi d_p^3 \rho_p}{6}\frac{dv_p}{dt} = \frac{\pi d_p^3 \rho_p}{6} g - 3\pi d_p \eta_g v_p \quad (1)$$

where v_p and g are velocitiy components of the particles in vertical direction and local gravitational acceleration, ρ_p is particle density, η_g is the viscosity of plasma gas, and d_p is the particle size.

By integrating Eq. (1), the velocity along the vertical direction will be positively correlated to particle size. Therefore, particles with larger sizes should rapidly pass through the high-temperature region in the center of plasma jet, leading to low heating efficiency. However, particles with smaller sizes will stay in the high-temperature region for long periods, easily reaching high temperatures. Based on our previous work [35,36], Fig. 8(a) schematically presents particle trajectory in laminar plasma jet. Although the movement of plasma torch should be considered in real condition, differences in particle trajectories based on particle size still existed. As spraying distance increased, the particle trajectory became quite different depending on particle size, and heating conditions also varied. S5 shows the particle size distribution during laminar plasma spraying at different spraying distances acquired by DPV-2000. The number of particles with sizes <25 μm decreased with

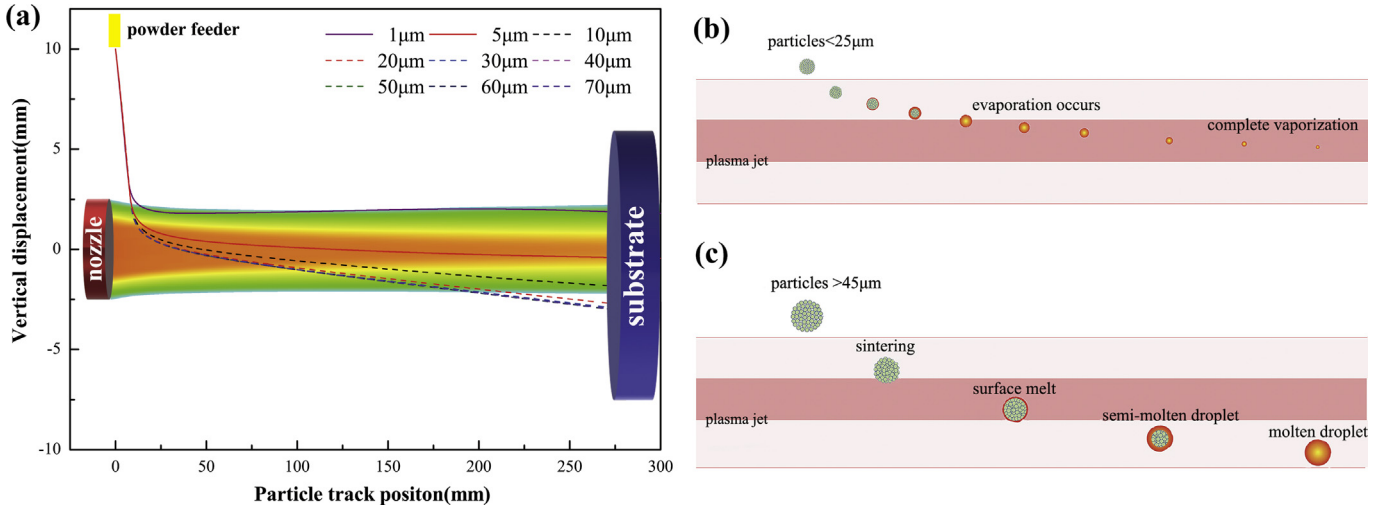

Fig. 8. Schematic representation of particle trajectory during laminar plasma spraying (a) and particle history in flight as a function of difference of diameter.

spraying distance while the number of particles with sizes >45 μm significantly increased. This indicated that size of the deposited unit changed with spraying distance, providing further confirmation of the proposed particles trajectory in flow. Reasonably, Fig. 8(b) and (c) display the history of LSCF particles with different particle sizes during plasma jet. Since the larger particles passed through the high-temperature central region rapidly, the plasma jet showed limited heating effect on the powders with sizes >45 μm. In addition, the melting of larger particles took more time in consideration of the influence of specific surface area of particles. The qualitative history of larger particles is shown in Fig. 8(c). On the other hand, small sized particles melted rapidly or even completely vaporized (Fig. 8(b)). Therefore, the deposition was dominated by well molten small particles, accompanied by partial vapor deposition (clusters) when the spraying distances were set to 150 mm and 200 mm due to the slow heating rate of larger particles. As spraying distance rose, large particles melted gradually. Hence, the coating mainly deposited by larger particles and contained typical lamellar structure at spraying distance of 250 mm. The deposition efficiency also enhanced rapidly with the spraying distance.

4.2. Impedance analyses and output characteristics of cells

The observed two impedance arcs at low and high frequencies in Fig. 7(d) indicate that the oxygen reduction reaction involves at least two electrochemical processes. In general, the high-frequency arc is related to charge transfer process, while the low-frequency arc is related to diffusion and adsorption/desorption process [37,38]. The equivalent circuit model was designed to correspond to $LR_o(R_{ct}CPE_{ct})(R_{gd}CPE_{gd})$ [38], where R_{ct} is related to the charge transfer resistance and R_{gd} is the gas diffusion resistance. More, L is wire inductance and R_o is the ohmic resistance. Table 2 lists the fitting results of polarization resistance for LSCF electrodes at different temperatures. As results of 750 °C show, the value of R_{ct} is comparable and R_{gd} value is quite different, indicating that the gas diffusion process becomes a limiting step. The improved gas diffusion efficiency can be related to the high vertical crack density.

As is shown in Fig. 9, oxygen reduction process for mixed conduction cathode (Fig. 9(a and b)) occurred within a distance (l_δ) from the electrolyte/cathode interface while the typical distances ranged from 3 to 5 μm [5]. In ideal case, the gas leakage rate of the cathode should be high so that oxygen can easily diffuse to the vicinity of reactive regions. Due to lamellar structure, the plasma

Table 2
Fitting results of electrochemical impedance (R_p, $\Omega \cdot cm^2$) for LSCF electrodes.

SD (mm)	650 °C			700 °C			750 °C		
	R_{ct}	R_{gd}	R_p	R_{ct}	R_{gd}	R_p	R_{ct}	R_{gd}	R_p
150	0.95	0.96	1.91	0.30	0.42	0.73	0.18	0.15	0.33
200	0.74	0.76	1.50	0.26	0.38	0.64	0.16	0.15	0.31
250	0.84	0.96	1.80	0.35	0.47	0.82	0.20	0.26	0.46

spray coating generally showed porosity ranging from 5% to 7% in APS coatings without pore formers [39]. The porosity was not high enough for cathode gas diffusion. In this study, the introduction of large numbers of vertical cracks (white lines in Fig. 9) led to significant reduction in polarization resistance of plasma-sprayed cathode obtained at spraying distances of 150 mm and 200 mm. Of all three groups of samples, the polarization resistance was the highest since the density of vertical cracks was relatively small at the spraying distance of 250 mm. The structured ALPS coatings with numerous vertical cracks might reduce the circuity of oxygen transport. The vertical cracks caused by high-temperature gradient significantly enhanced the transport of oxygen molecules (Fig. 9(c)).

Table 3 summarizes the cathode polarization resistance of LSCF and LSCF based composite cathodes prepared by other methods reported in the literature. The obtained cathode polarization resistances looked comparable with those of the cathode prepared screen printing [38], spin coating [40], plasma spraying [32,41] and other methods. The porosity of sprayed coatings was not as high as that obtained by wet-chemical-sintering methods due to porosity limitations of plasma spraying technology. However, the as-sprayed ALPS coatings were almost comparable in performance as other methods. Hence, ALPS looks promising for fabrication of intermediate temperature SOFCs. The proposed cathodes could be further improved by surface modification [42], addition of composite phase [43], and introduction of pore formers [44].

Whole cells with the structure of 430L||NiO/ScSZ||ScSZ||LSCF were tested. The output performances of the cells with LSCF coatings are shown in Fig. 10. Due to the plasma sprayed electrolyte coatings are difficult to be very dense [16,17,46], the open circuit voltages of the cell are ranging from 0.96 to 0.98 V. As shown in Fig. 10(a), the single cell for LSCF with SD = 200 mm as cathode shows the highest maximum power density among the three fuel

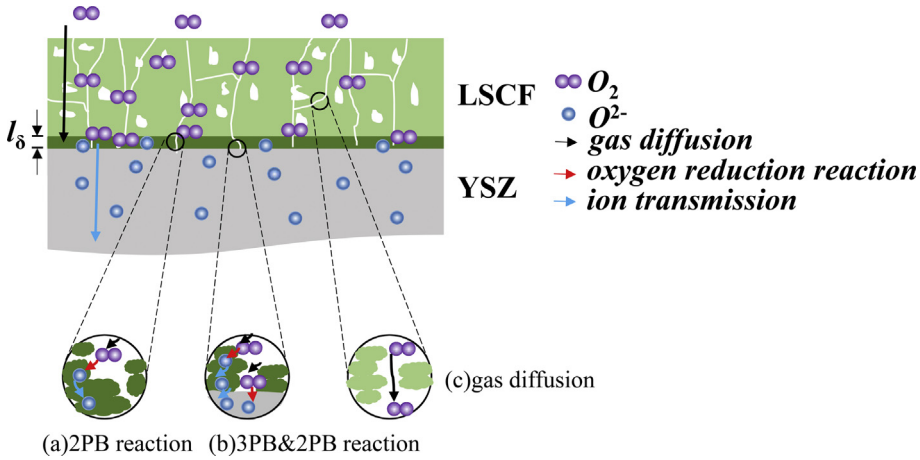

Fig. 9. Schematic diagram of the cathode electrochemical reactions.

Table 3
Cathode polarization (R_p, $\Omega \cdot cm^2$) properties reported in the literatures.

Cathode	Method	Electrolyte	650 °C	700 °C	750 °C	Reference
LSCF/GDC	APS	YSZ	–	–	0.83	[41]
LSCF	APS	ScSZ	–	1.2	0.541	[32]
LSCF/$La_2NiO_{4+\delta}$	Infiltration after APS	ScSZ	–	0.8	0.31	[32]
LSCF/SDC	APS nano-powders	YSZ			0.16	[39]
LSCF	ALPS	YSZ	1.5	0.64	0.31	this study
LSCF	Screen-printing	YSZ	2	0.745	0.345	[38]
LSCF	Spin-coating	SDC	1.28	0.85	0.33	[40]
LSCF/GDC	Infiltration	GDC	–	–	0.19	[45]
LSCF	Tape casting	SDC	–	–	0.15	[44]

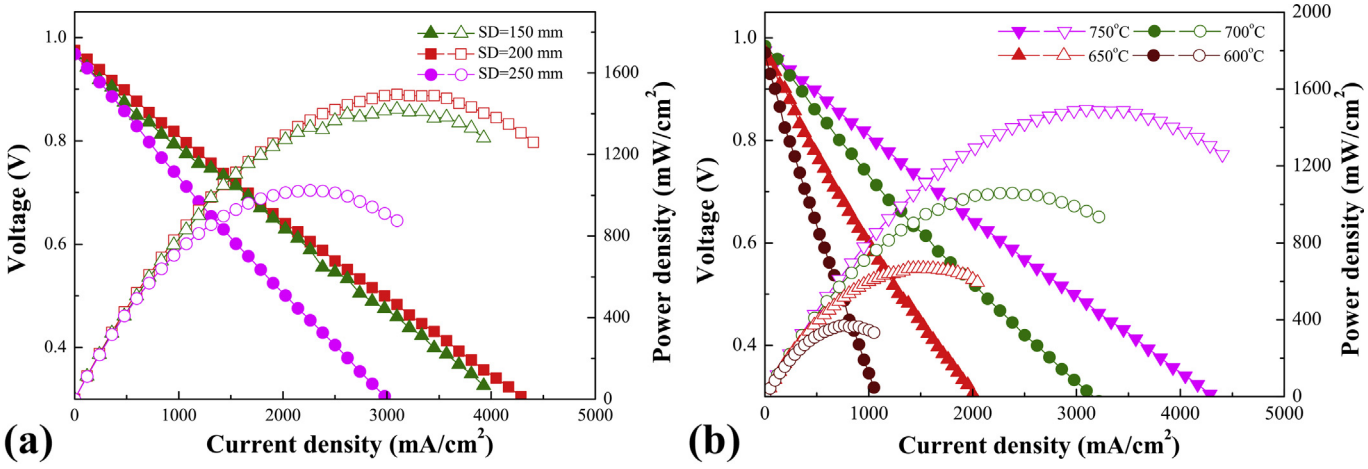

Fig. 10. Output performances of the cells with LSCF coatings: (a) cells with different cathodes at 750 °C; the SD = 200 mm sample measured at different temperatures.

cells tested. In addition, the maximum power densities values of the cell can reach 367, 667, 1059 and 1488 mW cm^{-2} at 600–750 °C (Fig. 10(b)). The result is consistent with the result of the impedance data.

5. Conclusions

LSCF coatings were successfully deposited by ALPS. The particles showed higher surface temperatures and lower velocities due to suitability of laminar plasma spraying. The sprayed coatings showed cluster-like surface morphologies with numerous vertical cracks on cross section at spraying distances of 150 mm and 200 mm. The effect of particle size led to variation in particle histories during plasma jet. Selective deposition based on particle size occurred at different spray distances, leading to formation of coatings with various structures. The coatings revealed lower polarization resistances when compared to LSCF coatings deposited by APS due to enhanced gas diffusion by vertical cracks. The output characteristics of the cells are also consistent with the impedance results. Overall, ALPS is a promising for the fabrication of SOFCs function layers.

Declaration of competing interest

The authors declare that they have no known competing financial interests or personal relationships that could have appeared to influence the work reported in this paper.

CRediT authorship contribution statement

Yue-Peng Wang: Conceptualization, Methodology, Investigation, Validation, Data curation, Writing - original draft, Formal analysis, Writing - review & editing. **Sen-Hui Liu:** Investigation, Validation. **Hui-Yu Zhang:** Investigation, Validation. **Cheng-Xin Li:** Conceptualization, Methodology, Supervision, Formal analysis, Writing - review & editing, Resources. **Shan-Lin Zhang:** Formal analysis, Writing - review & editing. **Guan-Jun Yang:** Formal analysis, Writing - review & editing. **Chang-Jiu Li:** Formal analysis, Writing - review & editing, Resources.

Acknowledgements

This work was supported by the National Key Research and Development Program of China (Basic Research Project, Grant No. 2017YFB0306100), the National Natural Science Foundation of China (Grant NO. 91860114), and the National Key Research and Development Program of China (China-USA Intergovernmental Cooperation Project, Grant NO. 2017YFE0105900).

Appendix A. Supplementary data

Supplementary data to this article can be found online at https://doi.org/10.1016/j.jallcom.2020.153865.

References

[1] F. Tietz, V.A.C. Haanappel, A. Mai, J. Mertens, D. Stöver, Performance of LSCF cathodes in cell tests, J. Power Sources 156 (2004) 20–22.
[2] V. Dusastre, J.A. Kilner, Optimisation of composite cathodes for intermediate temperature SOFC applications, Solid State Ionics Diffusion & Reactions 126 (1999) 163–174.
[3] Y. Chi, T. Li, B. Wang, Z. Wu, K. Li, Morphology, performance and stability of multi-bore capillary La 0.6 Sr 0.4 Co 0.2 Fe 0.8 O 3-δ oxygen transport membranes, J. Membr. Sci. 529 (2017) 224–233.
[4] C. Fu, K. Sun, N. Zhang, X. Chen, D. Zhou, Electrochemical characteristics of LSCF–SDC composite cathode for intermediate temperature SOFC, Electrochim. Acta 52 (2007) 4589–4594.
[5] S.B. Adler, Factors governing oxygen reduction in solid oxide fuel cell cathodes, Chem. Rev. 104 (2004) 4791–4843.
[6] L.D. Santos-Gómez, J. Hurtado, J.M. Porras-Vázquez, E.R. Losilla, D. Marrero-López, Durability and performance of CGO barriers and LSCF cathode deposited by spray-pyrolysis, J. Eur. Ceram. Soc. 38 (2018). S0955221918301614.
[7] C. Gao, Y. Liu, X. Kai, S. Jiao, R.I. Tomov, R.V. Kumar, Improve the catalytic property of La0.6Sr0.4Co0.2Fe0.8O3/Ce0.9Gd0.1O2 (LSCF/CGO) cathodes with CuO nanoparticles infiltration, Electrochim. Acta 246 (2017) 148–155.
[8] H.Y. Tu, Y. Takeda, N. Imanishi, O. Yamamoto, Ln 0.4Sr 0.6Co 0.8Fe 0.2O 3–δ (Ln=La, Pr, Nd, Sm, Gd) for the electrode in solid oxide fuel cells, Solid State Ionics 117 (1999) 277–281.
[9] D. Szymczewska, J. Karczewski, A. Chrzan, P. Jasinski, CGO as a Barrier Layer between LSCF Electrodes and YSZ Electrolyte Fabricated by Spray Pyrolysis for Solid Oxide Fuel Cells, Solid State Ionics, 2016. S0167273816305872.
[10] R. Hui, J.O. Berghaus, C. Decès-Petit, W. Qu, S. Yick, J.-G. Legoux, C. Moreau, High performance metal-supported solid oxide fuel cells fabricated by thermal spray, J. Power Sources 191 (2009) 371–376.
[11] B. Lin, W. Sun, K. Xie, Y. Dong, D. Dong, X. Liu, J. Gao, G. Meng, A cathode-supported SOFC with thin Ce0.8Sm0.2O1.9 electrolyte prepared by a suspension spray, J. Alloys Compd. 465 (2008) 285–290.
[12] A. Hospach, G. Mauer, R. Vaßen, D. Stöver, Columnar-structured thermal barrier coatings (TBCs) by thin film low-pressure plasma spraying (LPPS-TF), J. Therm. Spray Technol. 20 (2011) 116–120.
[13] S.-L. Zhang, C.-J. Li, C.-X. Li, G.-J. Yang, K. Huang, M. Liu, Liquid plasma sprayed nano-network La0.4Sr0.6Co0.2Fe0.8O3/Ce0.8Gd0.2O2 composite as a high-performance cathode for intermediate-temperature solid oxide fuel cells, J. Power Sources 327 (2016) 622–628.
[14] S.H. Liu, C.X. Li, L. Li, J.H. Huang, P. Xu, Y.Z. Hu, G.J. Yang, C.J. Li, Development of long laminar plasma jet on thermal spraying process: microstructures of zirconia coatings, Surf. Coating. Technol. 337 (2018). S0257897218300033.
[15] S.H. Liu, C.X. Li, H.Y. Zhang, S.L. Zhang, L. Li, P. Xu, G.J. Yang, C.J. Li, A novel structure of YSZ coatings by atmospheric laminar plasma spraying technology, Scripta Mater. 153 (2018) 73–76.
[16] S.-L. Zhang, C.-X. Li, C.-J. Li, G.-J. Yang, Z.-H. Han, Scandia-stabilized zirconia electrolyte with improved interlamellar bonding by high-velocity plasma spraying for high performance solid oxide fuel cells, J. Power Sources 232 (2013) 123–131.
[17] Y.P. Wang, J.T. Gao, W. Chen, C.X. Li, S.L. Zhang, G.J. Yang, C.J. Li, Development of ScSZ electrolyte by very low pressure plasma spraying for high-performance metal-supported SOFCs, J. Therm. Spray Technol. 29 (1–2) (2020) 223–231, https://doi.org/10.1007/s11666-019-00970-1.
[18] J. Harris, M. Qureshi, O. Kesler, Deposition of composite LSCF-SDC and SSC-SDC cathodes by axial-injection plasma spraying, J. Therm. Spray Technol. 21 (2012) 461–468.
[19] N. Orlovskaya, Y. Gogotsi, M. Reece, B. Cheng, I. Gibson, Ferroelasticity and hysteresis in LaCoO based perovskites, Acta Mater. 50 (2002) 715–723.
[20] L. Chen, G.J. Yang, C.X. Li, C.J. Li, Hierarchical formation of intrasplat cracks in thermal spray ceramic coatings, J. Therm. Spray Technol. 25 (2016) 959–970.
[21] S. Kuroda, T.W. Clyne, The quenching stress in thermally sprayed coatings, Thin Solid Films 200 (1991) 49–66.
[22] M. Wei, B. Wu, Determination of proper processing conditions of material surface heat treatment through finite element method, Surf. Coating. Technol. 201 (2006) 1519–1527.
[23] Y.Z. Lv, J.Y. Liu, Q.J. Xin, Wear process of SiC_p/Al-Si clad coating on the surface of aluminum alloy by laminar plasma jet, Heat Treat. Met. 30 (3) (2005) 31–33. http://en.cnki.com.cn/Article_en/CJFDTotal-JSRC200503009.htm.
[24] A. Kucuk, R.S. Lima, C.C. Berndt, Influence of plasma spray parameters on formation and morphology of ZrO2–8 wt% Y2O3 deposits, J. Am. Ceram. Soc. 84 (2010) 693–700.
[25] F.Y. Shen, K. Lu, Perovskite-type La0.6Sr0.4Co0.2Fe0.8O3, Ba0.5Sr0.5Co0.2-Fe0.8O3, and Sm0.5Sr0.5Co0.2Fe0.8O3 cathode materials and their chromium poisoning for solid oxide fuel cells, Electrochim. Acta 211 (2016) 445–452.
[26] A.A. Asadi, A. Behrouzifar, M. Iravaninia, T. Mohammadi, A. Pak, Preparation and oxygen permeation of La0.6Sr0.4Co0.2Fe0.8O3-δ (LSCF) perovskite-type membranes: experimental study and mathematical modeling, Ind. Eng. Chem. Res. 51 (2012) 3069–3080.
[27] P. Zeng, R. Ran, Z. Chen, H. Gu, Z. Shao, J.C.D.d. Costa, S. Liu, Significant effects of sintering temperature on the performance of La0.6Sr0.4Co0.2Fe0.8O3-δ oxygen selective membranes, J. Membr. Sci. 302 (2007) 171–179.
[28] M. Gao, C.J. Li, C.X. Li, S.Q. Fan, Effects of spray condition and annealing treatment on oxygen contents of thermally sprayed La0.5Sr0.5CoO3-δ coatings, J. Xi'an Jiaot. Univ. 44 (2010) 115–119.
[29] M. Gao, C.J. Li, C.X. Li, G.J. Yang, S.Q. Fan, Microstructure, oxygen stoichiometry and electrical conductivity of flame-sprayed Sm0.7Sr0.3CoO3-δ, J. Power Sources 191 (2009) 275–279.
[30] Y. Wang, H.B. Guo, Z.Y. Li, S.K. Gong, Segmented lanthanum cerium oxide thermal barrier coatings by atmospheric plasma spray, Surf. Eng. 25 (2009) 555–558.
[31] H.B. Guo, R. Vaßen, D. Stöver, Atmospheric plasma sprayed thick thermal barrier coatings with high segmentation crack density, Surf. Coating. Technol., 186 353-363.
[32] Y. Li, S.L. Zhang, C.X. Li, T. Wei, G.J. Yang, C.J. Li, M. Liu, La2NiO4+δ infiltration of plasma-sprayed LSCF coating for cathode performance improvement, J. Therm. Spray Technol. 25 (2016) 392–400.
[33] D. Marinha, L. Dessemond, J.S. Cronin, J.R. Wilson, S.A. Barnett, E. Djurado, Microstructural 3D reconstruction and performance evaluation of LSCF cathodes obtained by electrostatic spray deposition, Chem. Mater. 23 (2016) 5340–5348.
[34] J.O. Hinze, Turbulence: an Introduction to its Mechanism and Theory, McGraw-Hill Book Co., Inc., New York, 1959.
[35] S.H. Liu, J.P. Trelles, A.B. Murphy, L. Li, S.L. Zhang, G.J. Yang, C.X. Li, C.J. Li, Numerical simulation of the flow characteristics inside a novel plasma spray torch, J. Phys. D Appl. Phys. 52 (2019) 17.
[36] S.H. Liu, S.L. Zhang, C.X. Li, L. Li, J.H. Huang, J.P. Trelles, A.B. Murphy, C.J. Li, Generation of long laminar plasma jets: experimental and numerical analyses, Plasma Chem. Plasma Process. 39 (2019) 377–394.
[37] H.J. Men, N. Tian, Y.M. Qu, M. Wang, S. Zhao, J. Yu, Improved performance of a lanthanum strontium manganite-based oxygen electrode for an intermediate-temperature solid oxide electrolysis cell realized via ionic conduction enhancement, Ceram. Int. 45 (2019) 7945–7949.
[38] Q. Fu, K.N. Sun, N.Q. Zhang, X.D. Zhu, S.R. Le, D.R. Zhou, Characterization of electrical properties of GDC doped A-site deficient LSCF based composite cathode using impedance spectroscopy, J. Power Sources 168 (2007) 338–345.
[39] J. Harris, C. Metcalfe, M. Marr, J. Kuhn, O. Kesler, Fabrication and characterization of solid oxide fuel cell cathodes made from nano-structured LSCF–SDC composite feedstock, J. Power Sources 239 (2013) 234–243.
[40] K. Zhao, Q. Xu, D.P. Huang, M. Chen, B.H. Kim, Microstructure and electrode properties of La0.6Sr0.4Co0.2Fe0.8O3-δ spin-coated on Ce0.8Sm0.2O2–δ electrolyte, Ionics 17 (2011) 247–254.
[41] J. Harris, O. Kesler, Performance of metal-supported composite and single-phase cathodes based on LSCF and SSC, in: Ecs Meeting, 2011.
[42] X. Lou, S. Wang, Z. Liu, Y. Lei, M. Liu, Improving La0.6Sr0.4Co0.2Fe0.8O3–δ cathode performance by infiltration of a Sm0.5Sr0.5CoO3–δ coating, Solid

State Ionics 180 (2009) 1285–1289.
[43] W.G. Wang, M. Mogensen, High-performance lanthanum-ferrite-based cathode for SOFC, Solid State Ionics 176 (2005) 457–462.
[44] L. Nie, M. Liu, Y. Zhang, M. Liu, La0.6Sr0.4Co0.2Fe0.8O3−δ cathodes infiltrated with samarium-doped cerium oxide for solid oxide fuel cells, J. Power Sources 195 (2010) 4704–4708.
[45] Y. Liu, K. Chen, L. Zhao, B. Chi, J. Pu, S.P. Jiang, Performance stability and degradation mechanism of La0.6Sr0.4Co0.2Fe0.8O3-δ cathodes under solid oxide fuel cells operation conditions, Int. J. Hydrogen Energy 39 (2014) 15868–15876.
[46] S.-L. Zhang, C.-X. Li, C.-J. Li, Plasma-sprayed Y2O3-stabilized ZrO2Electrolyte with improved interlamellar bonding for direct application to solid oxide fuel cells, J. Fuel Cell Sci. Technol. 11 (2014), 031005.